Two-step antiferromagnetic transition and moderate triangular frustration in $Li_2Co(WO_4)_2$

I. Panneer Muthuselvam,[1] R. Sankar,[1] A. V. Ushakov,[2] G. Narsinga Rao,[1] Sergey V. Streltsov,[2,3] and F. C. Chou[1,4,5,*]

[1]*Center for Condensed Matter Sciences, National Taiwan University, Taipei 10617, Taiwan*

[2]*Institute of Metal Physics, Russian Academy of Science, S. Kovalevskaya Street 18, 620041 Ekaterinburg, Russia*

[3]*Ural Federal University, Mira Street 19, 620002 Ekaterinburg, Russia*

[4]*National Synchrotron Radiation Research Center, Hsinchu 30076, Taiwan*

[5]*Taiwan Consortium of Emergent Crystalline Materials, Ministry of Science and Technology, Taipei 10622, Taiwan*

(Received 19 October 2014; revised manuscript received 9 November 2014; published 21 November 2014)

We present a detailed investigation of the magnetic properties of the spin-$\frac{3}{2}$ system $Li_2Co(WO_4)_2$ by means of magnetic susceptibility and specific heat. Our experimental results show that in $Li_2Co(WO_4)_2$ short-range antiferromagnetic (AFM) correlations appear near $\chi_{max} \sim 11$ K and two successive long-range AFM phase transitions are observed at $T_{N1} \sim 9$ and $T_{N2} \sim 7$ K. The frustration factor $|\Theta|/T_{N1} \sim 3$ indicates that the system is moderately frustrated, which is identifiable by the broken triangular symmetry within both *ab* and *bc* planes for the triclinic crystal structure. The magnetic isotherm at temperatures below T_{N2} shows a field-induced spin-flop transition, and a complete H-T phase diagram for the two-step AFM system is mapped. *Ab initio* band-structure calculations suggest that the strongest exchange coupling does not correspond to the shortest Co-Co distance along the *a* axis but rather along the diagonal direction through a Co-O-W-O-Co supersuperexchange path within the *bc* plane.

DOI: 10.1103/PhysRevB.90.174430 PACS number(s): 75.30.Et, 75.10.−b

I. INTRODUCTION

Although one-dimensional (1D) antiferromagnetic (AFM) systems are not expected to show spin long-range ordering (LRO) as a result of strong quantum fluctuations, three-dimensional (3D) AFM LRO has been observed in most quasi-1D spin chain compounds because of the weak but nonzero interchain couplings. For gapped quasi-1D compounds, such as $PbNi_2V_2O_8$, $SrNi_2V_2O_8$, $TlCuCl_3$, and $Ni(C_5H_{14}N_2)_2N_3(PF_6)$, a strong magnetic field can destroy the gap and lead to the formation of an AFM ground state at low temperatures [1–4]. Cobalt-based low-dimensional magnetic systems often demonstrate behaviors of spin-flop (SF) and field-induced order-disorder transitions [5–10]. The most fascinating characteristic of low-dimensional systems is the observation of magnetization plateaus at high fields, i.e., magnetization could stabilize at a fraction of the saturated magnetization in quantum nature [11]. Two-step successive magnetic phase transition has been observed in 1D and two-dimensional (2D) Co spin systems, such as $Pb_3TeCo_3V_2O_{14}$ and $Ba_3CoNb_2O_9$ [8,10]. The common feature found in these two compounds is the persistent triangular symmetry of the Co spin network: either triangular tubing or planes. The comparative study between $Ba_3CoNb_2O_9$ and $Ba_3CoSb_2O_9$ suggests that the 2D triangular-lattice antiferromagnets (TLAFs) of uniaxial anisotropy exhibits a two-step magnetic phase transition, whereas a single transition takes place in systems with easy-plane anisotropy [8,12].

$Li_2Co(WO_4)_2$ crystalizes in a triclinic crystal structure of space group $P\bar{1}$ as shown in Fig. 1. The CoO_6 octahedra are corner shared with pairs of the WO_5 edge-shared pyramids, and Li ions are located in the interstitial sites. The Co-Co distances and Co-W-Co angles are summarized in Table I for the unit cell of $Li_2Co(WO_4)_2$ shown in Fig. 1(b). The CoO_6 octahedron is slightly distorted as indicated by the Co-O distances of 2.047, 2.099, and 2.164 Å. The WO_5 pyramids are inverted within each edge-sharing pair as shown in Fig. 1(c).

Recently, we found that $Li_2Co(WO_4)_2$ also possesses a two-step successive AFM transition similar to that of the examples cited above. To better understand the origin of this two-step successive magnetic transition, correlations to crystal dimensionality, spin anisotropy, triangular symmetry breaking, and the role of Dzyaloshinskii-Moriya interactions should all be carefully examined. The triclinic crystal structure of $Li_2Co(WO_4)_2$ provides a rare opportunity to investigate the origin of successive phase transitions found in the low-dimensional cobaltate system where Co spins could be viewed as two quasitriangles along two crystal axes.

In this paper, we present the investigation of the magnetic properties of $Li_2Co(WO_4)_2$. Short-range AFM correlations were found to result in the formation of the broad peak of $\chi_{max}(T)$ at $T \sim 11$ K, followed by a two-step AFM-like magnetic transition at $T_{N1} \sim 9$ and $T_{N2} \sim 7$ K. A two-step field-induced spin-flop transition was also observed in the magnetization isotherms below T_{N2}. Finally, we constructed a schematic phase diagram based on the results of the magnetic and specific heat measurements and found main exchange interaction parameters using band-structure calculations.

II. EXPERIMENTAL DETAILS

Polycrystalline $Li_2Co(WO_4)_2$ powder was prepared by a conventional solid-state reaction. Stoichiometric amounts of high purity (>99.95%) CoO, Li_2CO_3, and WO_3 were mixed and ground homogeneously using a mortar and pestle. The homogenized mixture of oxides was heated at 550 °C for 24 h in air. The calcined powder sample was pressed into pellets and heated up to 600 °C for 24 h and then 650 °C for 160 h in air with several intermediate grindings. The phase purity and structure refinement were confirmed by powder diffraction using synchrotron x rays of

*Corresponding author: fcchou@ntu.edu.tw

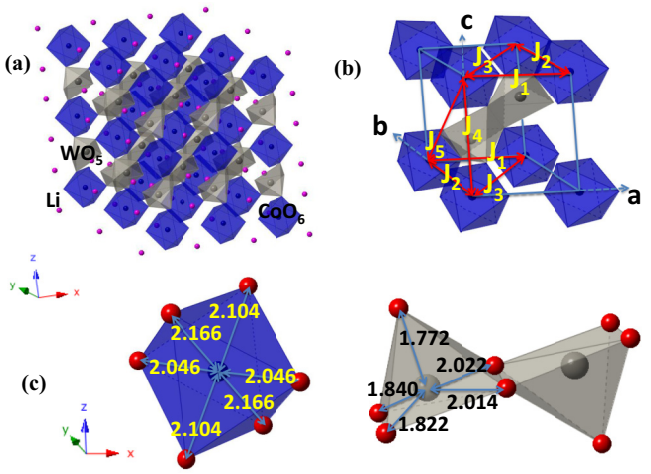

FIG. 1. (Color online) (a) Triclinic crystal structure of $Li_2Co(WO_4)_2$ shown with the CoO_6 octahedra in blue and the WO_5 pyramidal pairs in gray. (b) Magnetic exchange interactions (J_1-J_5) between the Co spins are shown, and the corresponding Co-Co distances are summarized in Table I. (c) Bond lengths in angstroms for the CoO_6 octahedra and the WO_5 pyramids.

$\lambda = 0.619$ Å (NSRRC, Taiwan) at room temperature. The Rietveld refinement of the single-crystal x-ray-diffraction pattern of the sample could be indexed to a triclinic crystal structure with the space group $P\bar{1}$ without any impurity phase. The refined lattice parameters of $Li_2Co(WO_4)_2$ are $a = 4.907\,24(7)$, $b = 5.618\,76(8)$, $c = 5.864\,95(8)$ Å, $\alpha = 70.720(1)^\circ$, $\beta = 88.542(1)^\circ$, $\gamma = 115.479(1)^\circ$, and $V = 135.110(3)$ Å^3, which are in good agreement with those reported in the literature [13]. These structural parameters were used in the *ab initio* band-structure calculations. The dc magnetization was measured using a superconducting quantum interference device vibrating-sample magnetometer (VSM) (Quantum Design, USA) under zero-field-cooled (ZFC) and field-cooled (FC) conditions. The heat capacity was measured using a standard relaxation method with a physical property measurement system (Quantum Design, USA).

III. CALCULATION DETAILS

The crystal structure data for the *ab initio* band-structure calculations were taken from the above-mentioned refinement results. The linearized muffin-tin orbitals method [14] was used in the calculations with the von Barth–Hedin exchange-correlation potential [15]. The strong Coulomb interaction in the $3d$ shell of the Co^{2+} ions was taken into account within the local spin-density approximation (LSDA) + U method [16]. The on-site Coulomb repulsion U and the intra-atomic Hund's exchange parameter J_H were chosen to be $U(\mathrm{Co}) = 7$ and $J_H(\mathrm{Co}) = 0.9$ eV [10,17]. We used a mesh of 96 k points in the full Brillouin zone during the course of the calculations.

The exchange-coupling integrals J were calculated for the Heisenberg model written as

$$H = \sum_{ij} J_{ij} \vec{S}_i \vec{S}_j, \tag{1}$$

where the summation runs twice over each pair. We utilized the Katsnelson and Liechtenstein exchange interaction parameters calculation procedure, where J is determined as a second derivative of the energy with respect to a small spin rotation [18]. The spin-orbit coupling was not taken into account.

The Co^{2+} ions form triangles along the ab and bc planes as shown in Fig. 1(b). The Co-Co bond lengths at room temperature for the Co quasiequilateral triangular unit within the ab plane are 4.902, 5.650, and 5.618 Å. Similarly, the Co triangular unit within the bc plane has slightly longer Co-Co distances of 5.618, 5.865, and 6.648 Å as seen in Fig. 1(b). The other Co-Co distances are much larger, thus the Heisenberg exchange interaction integrals were only estimated for the aforementioned bonds. For the calculations, we used the AFM structure in which the magnetic moments for the 4.902- and 5.618-Å Co-Co bonds were ordered antiferromagnetically, whereas those for the 5.65-Å Co-Co bond were ordered ferromagnetically. We also checked that the use of other AFM configurations does not change the calculation results (i.e., the J values). Spins along the c axis were taken to be antiferromagnetically ordered.

IV. RESULTS AND DISCUSSION

A. Magnetic susceptibility

Figure 2 shows homogeneous spin susceptibilities $\chi(T)$ as a function of temperature measured under an applied magnetic field of 1 T for $Li_2Co(WO_4)_2$. No hysteresis was observed between the ZFC and the FC measurement data. The $\chi(T)$ shows Curie-like behavior at high temperatures and reaches a rounded maximum at approximately $\chi_{\max} \sim 11$ K as shown in the inset of Fig. 2, which indicates the characteristic behavior of short-range AFM correlation for a low-dimensional spin system. Moreover, small but sharp drops in the $\chi(T)$ at approximately 9 and 7 K can be identified more clearly by $d(\chi T)/dT$ shown in the inset of Fig. 2 at $T_{N1} \sim 9$

TABLE I. Supersuperexchange paths J_1, J_2, J_3, J_4, and J_5 and their geometrical parameters.

	Distances Å					Bond angles (deg)		Torsion angle (deg)
Exchange parameters	Co-Co	Co-O	O···O	O-Co	Co-W-Co angle (deg)	Co-O···O	O···O-Co	Co-O···O-Co
$J_1 = 0.77$ K, AFM	4.907	2.187	2.663	2.089	85.01	88.53	135.11	93.72
$J_2 = 0.44$ K, AFM	5.618	2.189	2.929	2.085	103.24	100.52	165.39	31.75
$J_3 = 1.44$ K, AFM	5.650	2.084	2.737	2.089	101.17	114.048	155.03	41.54
$J_4 = 0.55$ K, AFM	5.865	2.085	2.823	2.188	106.40	144.95	126.44	11.94
$J_5 = 3.0$ K, AFM	6.648	2.189	2.383	2.189	127.70	158.16	158.16	180

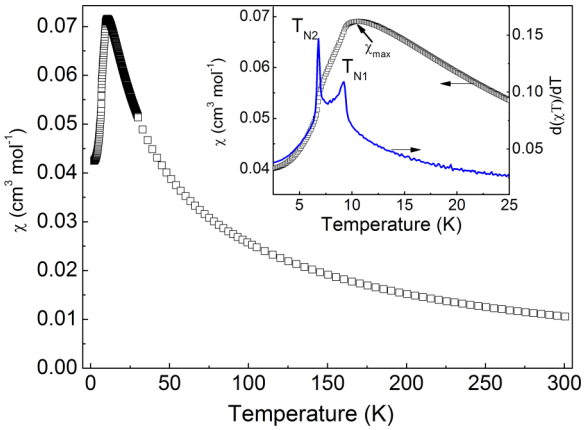

FIG. 2. (Color online) Temperature dependence of the magnetic susceptibility measured under an applied magnetic field of 1 T. The left axis of the inset highlights the low-temperature regime, and the right axis highlights the derivative $d(\chi T)/dT$.

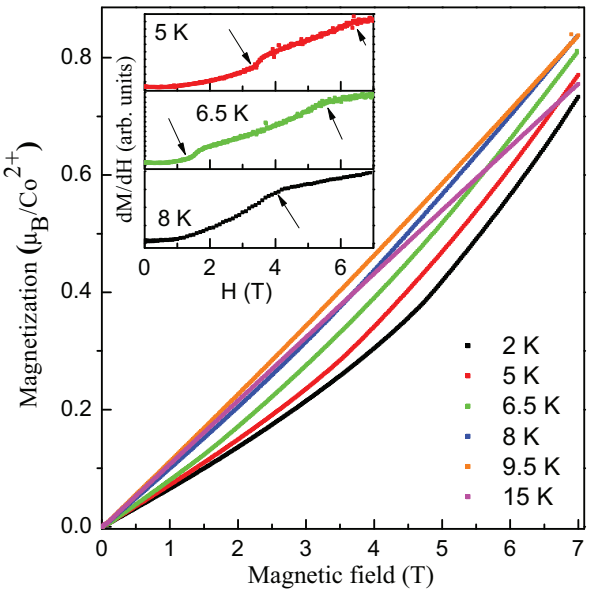

FIG. 3. (Color online) Field dependence of the magnetization measured at different temperatures for $Li_2Co(WO_4)_2$. The inset shows the derivative of the magnetization with respect to magnetic field.

and $T_{N2} \sim 7$ K. The preliminary neutron-powder-diffraction measurement results indicate that these phase transitions can be attributed to paramagnetic-to-incommensurate (IC) AFM LRO at $T_{N2} \sim 9$ K and IC-to-commensurate AFM LRO at $T_{N1} \sim 7$ K [19].

The $\chi(T)$ follows Curie-Weiss behavior well above 130 K, and the Curie-Weiss law fitting of $\chi = \chi_\circ + C/(T - \Theta)$ indicates a Curie constant of $C = 3.48$ cm^{-3} K^{-1} mol and a Curie-Weiss constant of $\Theta = -27$ K. The negative value of Θ suggests that the effective exchange interactions between Co^{2+} ions are AFM. The effective magnetic moment (μ_{eff}) was calculated to be $\sim 5.27\mu_B$, which is much larger than the expected $S = \frac{3}{2}$ spin-only value of $\sim 3.87\mu_B$ for Co^{2+} ($3d^7$ configuration in high spin state). The high value of the effective magnetic moment suggests the unquenched spin-orbit coupling for the high spin state of Co^{2+}. The obtained $\mu_{\text{eff}} \sim 5.2\mu_B$ is similar to those reported for several other Co^{2+}-based compounds [20–22]. The obtained g value derived from the Curie-Weiss constant is 2.72.

The spin frustration ratio $f = |\Theta|/T_{N1}$ was found to be ~ 3, which is indicative of moderate frustration taking place in the present system. Moderate frustration ($f \sim 2.8$) has been observed in $Pb_3TeCo_3V_2O_{14}$, which is characterized by a similar spin-lattice topology in addition to the resembling two-step successive AFM transition [10]. Based on the quasiequilateral triangular symmetry of the Co sublattices within both ab and bc planes [see Fig. 1(b)], it is reasonable to expect a moderate frustration among the Co spins if Ising-like anisotropy is considered on either plane.

Figure 3 shows the magnetization as a function of applied magnetic field measured at different temperatures. The $M(H)$ curves show nonlinear behavior with the applied magnetic field. At temperatures below T_{N2}, an abrupt change in slope in the magnetization is observed above certain critical magnetic fields (shown in the inset of Fig. 3). Interestingly, a two-step behavior is observed in the magnetization isotherms below T_{N2}, which is strongly evidenced by the dM/dH derivative shown in the inset. The change in dM/dH slope could be attributed to the field-induced magnetic phase transition or the spin-flop reorientation. Based on the slope increase in $M(H)$ above the critical fields, the first transition can be attributed to a spin-flop transition in which the magnetic field overcomes the spin anisotropy and the AFM spins flop. Judging from the $M(H)$ slope decrease in the second step for $M(H)$ below T_{N2} and the first step for $M(H)$ above T_{N2}, the field-induced transition (FIT) cannot be assigned to a spin-flop transition. No hysteresis or remnant magnetization is observed in zero field. Because it is difficult to determine the easy axis in the AFM state using polycrystalline samples and the magnetization does not saturate up to 7 T, high-field experiments on a single-crystal sample are necessary for the detailed analysis, especially for the second step observed in $M(H)$.

To further clarify the field-induced transition, we have performed magnetic susceptibility measurements in different applied magnetic fields (H). Figure 4 shows the temperature dependence of the magnetization under different fields, and derivative $d(\chi T)/dT$ is presented in the inset. With increasing field, $\chi_{\max}$ shifts to lower temperatures. In addition, both T_{N2} and T_{N1} shift to lower temperatures (inset of Fig. 4) at higher fields, although the peaks in $d(\chi T)/dT$ become significantly broader at high fields. The decrease in T_{N2} and T_{N1} is expected for a 3D TLAF with easy-axis anisotropy when both interlayer and intralayer AFM exchange interactions are on the same order of magnitude [23,24]. Recently, similar behavior has also been observed in $Ba_3CoNb_2O_9$ [8]. However, both T_{N1} and T_{N2} increase with increasing magnetic field when $H \perp c$ in $CsNiCl_3$ where the AFM interlayer exchange interaction is much larger than the intralayer magnetic coupling [25]. It is clear that the magnetic field is effective for lifting the degeneracy of the spin structure with a frustrated triangular geometry. The $Li_2Co(WO_4)_2$ with triclinic crystal symmetry possesses a Co spin lattice with a quasiequilateral triangular geometry, which could explain the reason why the onset of the AFM is so sensitive to the applied field.

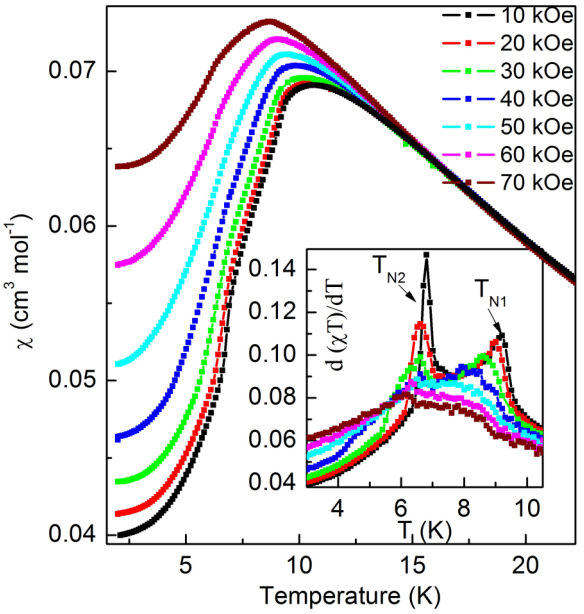

FIG. 4. (Color online) Temperature dependence of the magnetic susceptibility at various applied magnetic fields with $d(\chi T)/dT$ shown in the inset.

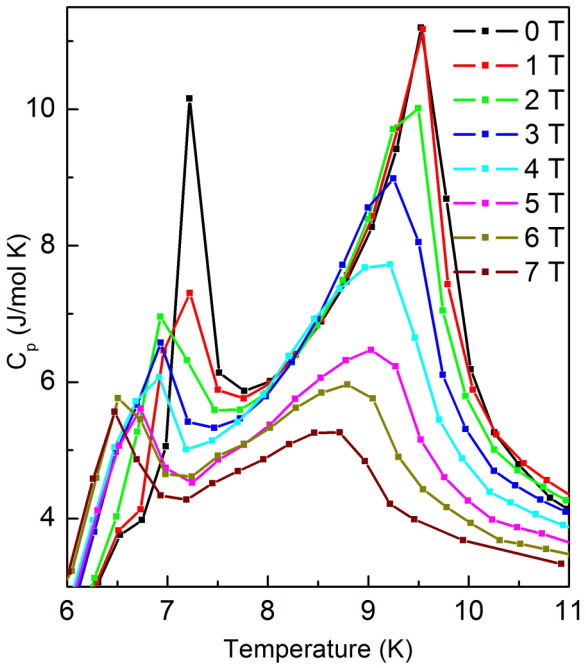

FIG. 6. (Color online) C_P versus T for different external magnetic fields.

B. Specific heat

Figure 5 shows the specific heat C_P as a function of temperature in zero field where two anomalies are observed at $T_{N1} \sim 7.2$ and $T_{N2} \sim 9.5$ K. These results provide strong evidence that the two successive phase transitions are both of 3D LRO and are consistent with the AFM nature inferred from the spin susceptibility measurements. The $C_P(T)$ data are fitted using $C_P/T = \alpha + \beta T^2$ above 15 K to estimate the lattice and spin contributions, which yield $\alpha = 0.127\ \mathrm{J\,mol^{-1}\,K^{-2}}$ and $\beta = 2.84 \times 10^{-4}\ \mathrm{J\,mol^{-1}\,K^{-4}}$. Because $Li_2Co(WO_4)_2$ is an insulator, α is assumed to originate from magnetic contributions only. The magnetic specific heat (C_m) is obtained after subtracting the lattice contribution (βT^3) from the total C_P. C_m is found to follow a linear dependence of T^3 below T_{N2}, which is indicative of AFM magnon excitations in the ordered state [26]. The magnetic entropy (S_m) is estimated through integrating C_m/T as a function of temperature as shown in Fig. 5. The S_m increases with increasing temperature and saturates to $10.45\ \mathrm{J\,mol^{-1}\,K^{-1}}$ above ~52 K, which suggests the measured saturated entropy is approximately 91% of the calculated value of the total spin entropy of $R\ln(2S+1) = 11.53\ \mathrm{J\,mol^{-1}\,K^{-1}}$ ($R = 8.314\ \mathrm{J\,K^{-1}\,mol^{-1}}$) for spin $= \frac{3}{2}$. However, the entropy gain at T_{N1} is only ~1/3 of the total spin entropy for spin $\frac{3}{2}$, which suggests that $Li_2Co(WO_4)_2$ could be characterized as a quasi-low-dimensional spin system, i.e., the remaining spin entropy has to be gradually acquired by the short-range magnetic correlation in a wide range of temperatures above T_{N1}.

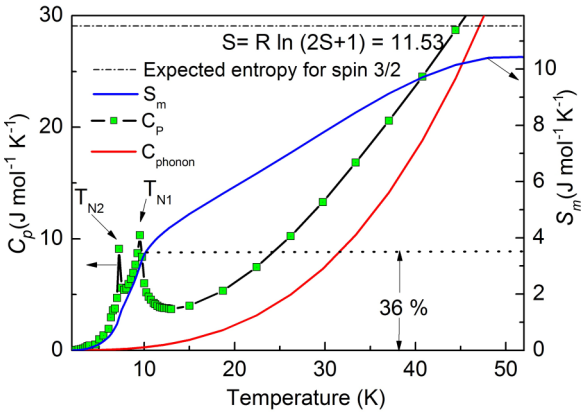

FIG. 5. (Color online) Specific heat as a function of temperature (left, y axis) and magnetic entropy S_m versus T (right, y axis).

C_P measurements in different applied fields have been performed and are shown in Fig. 6. With increasing H, both T_{N1} and T_{N2} peaks shift toward lower temperatures. In addition, the amplitude of the peaks also decreases with increasing H. These results are consistent with the common features of AFM magnetic systems. Although the T_{N1} peak becomes dramatically rounded with increasing H above ~4 T, the T_{N2} peaks are not completely suppressed up to 70 kOe, and no significant broadening occurs except for the 1/2 to 1/3 intensity reduction. The broadening of T_{N1} under high fields suggests that the magnetic field could suppress the interplane coupling for the original 3D LRO through moderate frustration, which has also been reflected in the magnetic susceptibilities shown in Fig. 4. From this point of view, the T_{N1} peak broadening in the field (above T_{N2}) could be attributed to a moderate field-induced order-disorder transition. This result was also reflected in the ~1/3 spin entropy gain at T_{N1} (see Fig. 5), similar to that obtained in the quasi-1D system of $BaCo_2V_2O_8$ [5]. However, the persistently sharp character of T_{N2} in high fields suggests that LRO exists below T_{N2}, although it is suppressed at a lower onset.

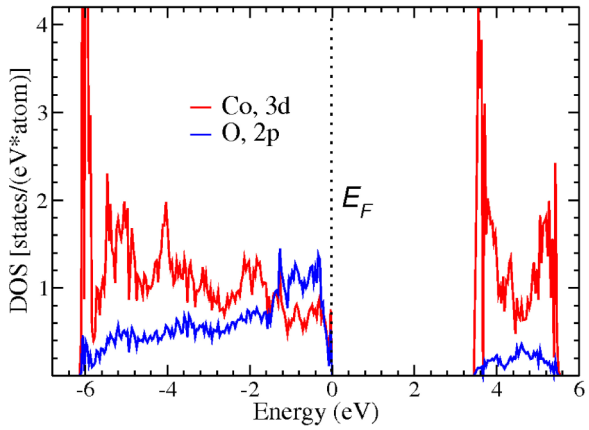

FIG. 7. (Color online) The total densities of Co-d and O-2p states in $Li_2Co(WO_4)_2$. The Fermi energy is in zero.

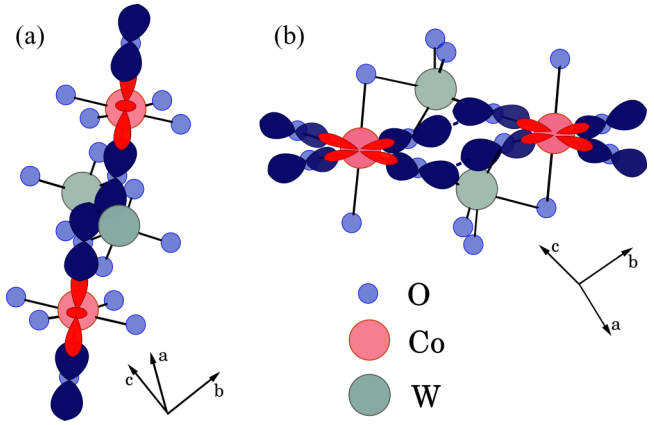

FIG. 8. (Color online) The schematic of the exchange paths for the largest exchange integrals with the Co-Co bond lengths 6.648 and 5.650 Å.

C. *Ab initio* calculations

In the LSDA + U calculations, $Li_2Co(WO_4)_2$ was found to be an insulator with an energy gap of $E_g \sim 3.5$ eV. The electronic density of states are shown in Fig. 7. The top of the valence band is formed by the Co-d and O-2p states, whereas the bottom of the conduction band mostly has Co-3d character. The width of the valence band is quite large, ~6 eV. The local magnetic moments on the Co^{2+} were found to be $2.75\mu_B$, which are in agreement with the $3d^7$ high spin configuration.

The calculated exchange coupling parameters for $Li_2Co(WO_4)_2$ are presented in Table I. We estimated the Curie-Weiss temperature as $\Theta = \frac{2}{3}\sum_i J_i S(S+1)$, where $S = \frac{3}{2}$ for the spin moment of the Co^{2+} ion, and found that $\Theta = -24.8$ K. This value is in good agreement with the experimental estimation of $\Theta = -27$ K given above, which shows that the results of the calculations are reliable.

Based on the coupling constants estimated above, the largest constant (J_5) is approximately twice as large as J_3. Hence the system could be considered a set of coupled spin chains, running along the J_5 direction as shown in Fig. 1(b) and Table I. Two substantial exchange integrals J_3 and J_5 correspond to Co-Co distances of 5.650 and 6.648 Å, respectively. It is interesting to find that the strongest exchange coupling J_5 does not correspond to the shortest Co-Co bond lengths but rather the longest among J_i and the largest bond angle between Co-W-Co.

Each CoO_6 octahedron in $Li_2Co(WO_4)_2$ at room temperature is slightly elongated along one of the directions as shown in Fig. 1(c). This removes the degeneracy in the t_{2g} shell, and one of the t_{2g} orbitals (xy in the local coordinate system, where z corresponds to the longest Co-O bond) goes higher in energy. As a result, the xy, $3z^2$-r^2, and x^2-y^2 orbitals are half-filled and magnetically active for the Co^{2+} ions in the HS configuration.

The analysis of the partial contributions shows that the largest contribution to J_5 arises from the overlap between $3z^2$-r^2 orbitals centered on different sites. Structurally, it is clearly seen that this result may be attributed to the supersuperexchange interaction via p orbitals of O in the WO_4 group as shown in Fig. 8(a). The second strongest exchange integral J_3 belongs to the Co triangular plane that results from the overlap of the x^2-y^2 orbitals of Co with the p orbitals of O via the WO_4 group as shown in Fig. 8(b).

According to the Goodenough-Kanamori-Andersen rules, both of these exchange constants (J_3 and J_5) should be AFM [27,28], the strong AFM exchange interaction is expected when the partially filled d orbitals overlap with a nonmagnetic ion angle of 180°, whereas weak ferromagnetic interaction is exhibited when the angle is close to 90°. The other exchange constants are much smaller because the CoO_6 octahedra are isolated from each other by the Li and W ions. Even for the shortest Co-Co bond 4.90 Å, it is difficult to find a possible exchange path with the large overlap of Co-3d orbitals centered on different sites.

Upon examining the copper oxide compounds with a supersuperexchange interaction route, Koo *et al.* proposed that the supersuperexchange strength of M-O···O-M increases with an increasing bond angle of M-O-O and decreases with O···O distance [29]. In particular, the supersuperexchange interaction is non-negligible only when the O···O distance is close to or shorter than the van der Waals distance (2.8 Å), and the M-O···O angles are near 160° [30]. The bond lengths and bond angles are summarized in Table I. From Table I, we can conclude that J_5 should be the largest because of the shortest O···O (2.383-Å) distance and the largest Co-O···O angle of 158.16°. Generally, the supersuperexchange via several O ions is often found to be a strong exchange interaction [10,30]. The second largest exchange interaction is expected to be J_3 because of the intermediate O···O distance and Co-O···O and O···O-Co bond angles. J_2 and J_4 could be the weakest because the O···O distances are slightly larger than the van der Waals distance of 2.8 Å. These findings based on bond length and bond angle alone are in good agreement with those obtained from our theoretical calculations shown above.

D. Phase diagram

Since the slope of $M(H)$ isotherms below T_{N2} increases with field and the C_P peaks at T_{N2} remain sharp to indicate a persistent LRO, the first slope change in $M(H)$ for temperatures below T_{N2} (see Fig. 3) must result from a spin-flop transition. A spin-flop transition occurs when the applied

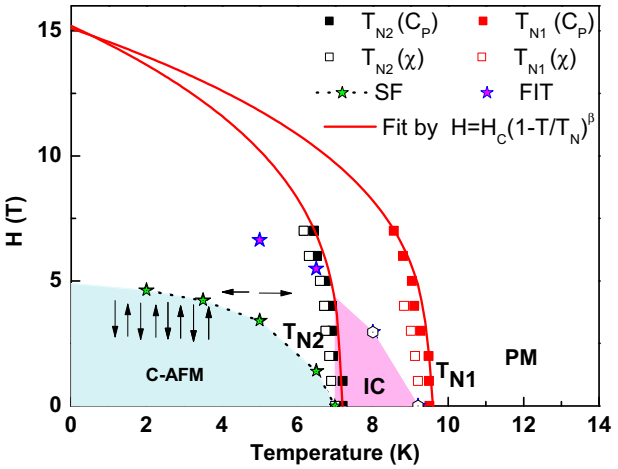

FIG. 9. (Color online) Phase diagram constructed from susceptibility (open symbol), M versus H (star symbols) and specific heat measurements (closed symbol). The solid lines are power-law fitting, and the dashed lines are guides for the eye.

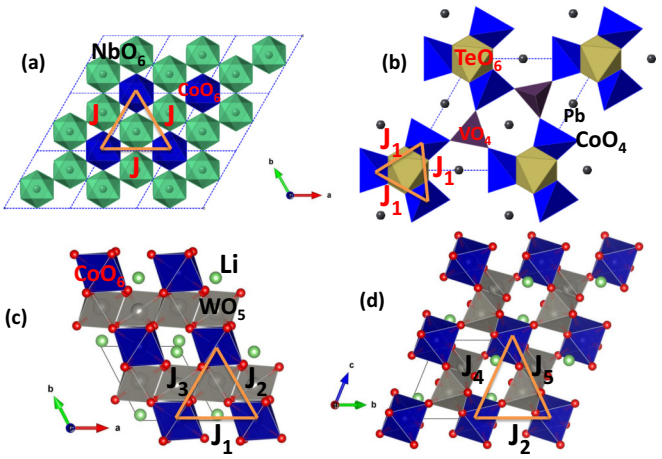

FIG. 10. (Color online) The crystal structure along the ab plane for (a) $Ba_3CoNb_2O_9$ and (b) $Pb_3TeCo_3V_2O_{14}$. (c) ab plane and (d) bc planes of $Li_2Co(WO_4)_2$. All J_i coupling constants are defined following Refs. [8,10] and Fig. 1.

field is high enough to overcome the on-site spin anisotropy, but the AFM LRO is preserved after all spins are flopped perpendicular to the field direction. However, as seen in Fig. 3, there exists a second slope change for $M(H)$ below T_{N2}, which cannot be attributed to an additional spin-flop transition due to a smaller slope, thus a canted ferromagnetic phase transition is possible.

Figure 9 shows the H-T phase diagram, constructed from the $\chi(H,T)$, $M(H,T)$, and $C_P(H,T)$ measurement results up to 7 T of the VSM field limit. Both SF and FIT are identified from the $M(H)$ isotherms through their derivatives. It is not expected for one AFM ordering to have two consecutive spin-flop transitions along one axis through single anisotropy gain. Furthermore, the second slope below T_{N2} is smaller, which goes against the definition of spin-flop transition. However, it is likely that the second slope change for $M(H)$ below T_{N2} indicates an onset of a canted ferromagnetic transition from the AFM phase after all of the spins are flopped.

Using the $T_N(H)$ values obtained from the $C_P(T)$ data at various fields, the critical field H_c and exponent β can be calculated through a power-law fitting of $H/H_c = (1 - T/T_c)^{\beta}$. This yields $H_c = 15.3$ T for T_{N2}, $H_c = 15.1$ T for T_{N1}, and $\beta = 1/3$ as expected from the mean-field theory prediction. Between $T_{N2} < T < T_{N1}$, a single spin-flop transition is identified, which could be attributed to the spin-flop transition of an AFM phase below T_{N1}. Preliminary neutron-diffraction studies indicate that the AFM phase below T_{N1} is an incommensurate AFM phase, and the AFM phase below T_{N2} is commensurate, the details of which will be reported elsewhere [19].

It is worthwhile to compare the H-T phase diagrams of $Li_2Co(WO_4)_2$ with two other cobaltate systems $Ba_3CoNb_2O_9$ and $Pb_3TeCo_3V_2O_{14}$, which exhibit similar two-step AFM transitions [8,10]. The quasiequilateral triangular arrangements of Co ions in $Li_2Co(WO_4)_2$, $Ba_3CoNb_2O_9$, and $Pb_3TeCo_3V_2O_{14}$ are depicted in Fig. 10. The spin structure of $Ba_3CoNb_2O_9$ can be extracted from the layers of Co spins within the CoO_6 octahedra in the triangular lattice, and the weak interlayer coupling is obtained through the double corner-sharing NbO_6 layers. An easy-axis anisotropy and two-step AFM transition (near $T_{N1} = 1.39$ and $T_{N2} = 1.13$ K) in $Ba_3CoNb_2O_9$ was identified, which strongly suggests that the triangular geometric frustration is lifted via possible magnetophonon coupling, as revealed by the 3D LRO of AFM in steps. The structure of $Pb_3TeCo_3V_2O_{14}$ consists of quasi-1D structure in which CoO_6 octahedra form a unique triangular tubing along the c direction with the two-step AFM transitions found near $T_{N1} = 9$ and $T_{N2} = 6$ K. It is noted that the CoO_6 trimer within each triangular tubing is coupled through a supersuperexchange route via corner sharing with the TeO_6 octahedra along the c direction, and these CoO_6 trimers within the ab plane also form a superlattice of triangular lattices. The stronger intrachain coupling could lead to the first incommensurate AFM ordering at T_{N1} that eventually orders as a commensurate AFM below T_{N2}. Although $Li_2Co(WO_4)_2$ does not possess a perfect triangular symmetry compared to the other two cobaltates, the triclinic symmetry of the Co spins can be simplified as two quasiequilateral triangles of J_1-J_2-J_3 within the ab plane and J_2-J_4-J_5 within the bc plane as illustrated in Fig. 1 with the Co-Co distances summarized in Table I. The unique coordination between CoO_6 bridged with WO_4 pairs could also compete with the two nearly orthogonal ($\beta = 91.46^\circ$) quasitriangles. We believe that the common character of the nearly identical two-step AFM transitions found in these three samples may be attributed to the magnetophonon coupling of the bridging polyhedra, which preferably lifts the moderate geometric frustration of the triangular Co spins.

V. CONCLUSION

To summarize, $Li_2Co(WO_4)_2$ exhibits a two-step successive three-dimensional antiferromagnetic transition at $T_{N1} \sim 9$ and $T_{N2} \sim 7$ K. The data collected in $\chi(H,T)$, $M(H,T)$, and $C_P(H,T)$ measurements were used to establish the magnetic phase diagram of $Li_2Co(WO_4)_2$. This diagram was compared with that of two other cobaltate systems $Ba_3CoNb_2O_9$ and

$Pb_3Co_3TeAs_2O_{14}$ with a triangular motif of the crystal structure in which a similar two-step AFM transition was found. The spin frustration ratio $f = |\Theta|/T_N \sim 3$ indicates that the system is moderately frustrated, which could break the triangular symmetry in both *ab* and *bc* planes for Co spins in the unique triclinic crystal structure. The analysis of the results of the LSDA + U calculations allowed finding the strongest exchange interactions, which is between fifth nearest neighbors. This is the supersuperexchange coupling via two oxygen ions, which results in the formation of AFM chains forming a triangular network. Similar long-range exchange interactions were found in other Co^{2+}-based systems having two-step AFM transitions: $Ba_3CoNb_2O_9$ and $Pb_3Co_3TeAs_2O_{14}$.

ACKNOWLEDGMENTS

The results of experimental measurements were obtained by I.P.M., R.S., G.N.R., and F.C.C. and were supported by MOST under Project No. MOST-102-2119-M-002-004. The results of the theoretical calculations: electronic structure and magnetic parameters were obtained by A.V.U. and S.V.S. and were supported by a grant from the Russian Scientific Foundation (Project No. 14-22-00004).

[1] N. Tsujii, O. Suzuki, H. Suzuki, H. Kitazawa, and G. Kido, Phys. Rev. B **72**, 104402 (2005).
[2] A. K. Bera, B. Lake, A. T. M. N. Islam, B. Klemke, E. Faulhaber, and J. M. Law, Phys. Rev. B **87**, 224423 (2013).
[3] Z. Honda, H. Asakawa, and K. Katsumata, Phys. Rev. Lett. **81**, 2566 (1998).
[4] A. Oosawa, M. Ishii, and H. Tanaka, J. Phys.: Condens. Matter **11**, 265 (1999).
[5] Z. He, T. Taniyama, T. Kyomen, and M. Itoh, Phys. Rev. B **72**, 172403 (2005).
[6] Z. He, T. Taniyama, and M. Itoh, Phys. Rev. B **73**, 212406 (2006).
[7] Z. He, J. I. Yamaura, Y. Ueda, and W. Cheng, J. Am. Chem. Soc. **131**, 7554 (2009).
[8] K. Yokota, N. Kurita, and H. Tanaka, Phys. Rev. B **90**, 014403 (2014).
[9] N. Mohapatra, K. K. Iyer, S. D. Das, B. A. Chalke, S. C. Purandare, and E. V. Sampathkumaran, Phys. Rev. B **79**, 140409(R) (2009).
[10] M. M. Markina, B. V. Mill, E. A. Zvereva, A. V. Ushakov, S. V. Streltsov, and A. N. Vasiliev, Phys. Rev. B **89**, 104409 (2014).
[11] A. Honecker, J. Schulenburg, and J. Richter, J. Phys.: Condens. Matter **16**, S749 (2004).
[12] T. Susuki, N. Kurita, T. Tanaka, H. Nojiri, A. Matsuo, K. Kindo, and H. Tanaka, Phys. Rev. Lett. **110**, 267201 (2013).
[13] M. Álvarez-Vega, J. Rodríguez-Carvajal, J. G. Reyes-Cárdenas, A. F. Fuentes, and U. Amador, Chem. Mater. **13**, 3871 (2001).
[14] O. K. Andersen and O. Jepsen, Phys. Rev. Lett. **53**, 2571 (1984).
[15] U. von Barth and L. Hedin, J. Phys. C: Solid State Phys. **5**, 1629 (1972).
[16] V. Anisimov, F. A. Aryasetiawan, and A. Liechtenstein, J. Phys.: Condens. Matter **9**, 767 (1997).
[17] L. V. Nomerovannaya, A. A. Makhnev, S. V. Streltsov, I. A. Nekrasov, M. A. Korotin, S. V. Shiryaev, G. L. Bychkov, S. N. Barilo, and V. I. Anisimov, J. Phys.: Condens. Matter **16**, 5129 (2004).
[18] M. I. Katsnelson and A. I. Lichtenstein, Phys. Rev. B **61**, 8906 (2000).
[19] C. W. Wang, I. P. Muthuselvam, R. Sankar, S. K. Karna, M. Avdeev, and F. C. Chou (unpublished).
[20] M. C. Viola, M. J. Martínez-Lope, J. A. Alonso, J. L. Martínez, J. M. De Paoli, S. Pagola, J. C. Pedregosa, M. T. Fernández-Díaz, and R. E. Carbonio, Chem. Mater. **15**, 1655 (2003).
[21] G. Nakayama, S. Hara,, H. Sato, Y. Narumi, and H. Nojir, J. Phys.: Condens. Matter **25**, 116003 (2013).
[22] Z. He, D. Fu, T. Kyomen, T. Taniyama, and M. Itoh, Chem. Mater. **17**, 2924 (2005).
[23] M. L. Plumer, K. Hood, and A. Caille, Phys. Rev. Lett. **60**, 45 (1988).
[24] M. L. Plumer, A. Caille, and K. Hood, Phys. Rev. B **39**, 4489 (1989).
[25] P. B. Johnson, J. A. Rayne, and S. A. Friedberg, J. Appl. Phys. **50**, 1853 (1979).
[26] J. A. Gotaas, J. S. Kouvel, and T. O. Brun, Phys. Rev. B **32**, 4519 (1985).
[27] J. B. Goodenough, Phys. Rev. **100**, 564 (1955).
[28] J. Kanamori, J. Phys. Chem. Solids **10**, 87 (1959).
[29] H.-J. Koo, D. Dai, and M.-H. Whangbo, Inorg. Chem. **44**, 4359 (2005).
[30] M.-H. Whangbo, H.-J. Koo, D. Dai, and D. Jung, Inorg. Chem. **42**, 3898 (2003).